
Article:
Peters, Daniel T, Fung, Herman Kh, Levdikov, Vladimir M et al. (7 more authors) (2016) Human Lin28 forms a high-affinity 1:1 complex with the 106~363 cluster miRNA miR-363. Biochemistry. 5021−5027. ISSN 1520-4995

https://doi.org/10.1021/acs.biochem.6b00682

Human Lin28 forms a high-affinity 1:1 complex with the 106~363 cluster miRNA miR-363

Journal:	*Biochemistry*
Manuscript ID	bi-2016-00682u.R1
Manuscript Type:	Article
Date Submitted by the Author:	n/a
Complete List of Authors:	Peters, Daniel; Newcastle University Faculty of Medical Sciences, Institute of Cell and Molecular Biosciences Fung, Herman; University of York, Biology Levdikov, Vladimir; University of York, Chemistry Irmscher, Tobias; University of York, Chemistry Warrander, Fiona; University of York, Chemistry Greive, Sandra; University of York, Chemistry Kovalevskiy, Oleg; MRC Laboratory of Molecular Biology, Structural Studies Division Isaacs, Harry; University of York, Biology Coles, Mark; University of York,, Centre for Immunology and Infection, Department of Biology Antson, Alfred; University of York, Chemistry

Human Lin28 forms a high-affinity 1:1 complex with the 106~363 cluster miRNA miR-363

Daniel T Peters[†,‡], Herman KH Fung[†,§], Vladimir M Levdikov[†], Tobias Irmsche[†], Fiona C. Warrander[§], Sandra J. Grieve[†], Oleg Kovalevskiy[†,//], Harry V. Isaacs[§], Mark Coles[§], Alfred A. Antson[†]*

[†] York Structural Biology Laboratory, Department of Chemistry, University of York, York, YO10 5DD, United Kingdom

[§] Department of Biology, University of York, York, YO10 5DD, United Kingdom

Corresponding Author

* E-mail: fred.antson@york.ac.uk. Telephone: (44) 1904 328255.

Present Addresses

[‡] Institute of Cell and Molecular Biosciences, Medical School, Cookson Building, Framlington Place, Newcastle University, NE2 4HH, United Kingdom

[//] Structural Studies Division, MRC Laboratory of Molecular Biology, Francis Crick Avenue, Cambridge CB2 0QH, United Kingdom

Funding Sources

This work was supported by the Wellcome Trust (WT098230). DTP was funded by a PhD studentship from the Yorkshire Cancer Research and HKHF is supported by a PhD studentship from the Wellcome Trust (WT095024MA).

ABBREVIATIONS

CSD, cold shock domain; ZnK, zinc knuckle; miRNA, microRNA; *Xenopus, Xenopus tropicalis*; *Mmu*, *Mus musculus*; MBP, maltose binding protein; His-MBP-Lin28TT, His-MBP-Lin28 with truncated termini; SEC-MALLS, Size exclusion chromatography coupled with multi-angle laser-light scattering.

ABSTRACT

Lin28A is a post-transcriptional regulator of gene expression that interacts with and negatively regulates the biogenesis of let-7 family miRNAs. Recent data suggested that Lin28A also binds the putative tumour suppressor miR-363, a member of the 106~363 cluster of miRNAs. Affinity toward this miRNA and the stoichiometry of the protein-RNA complex are unknown. Characterisation of human Lin28's interaction with RNA has been complicated by difficulties in producing stable RNA-free protein. We have engineered a maltose binding protein fusion with Lin28, which binds let-7 miRNA with a K_d of 54.1 ± 4.2 nM, in agreement with previous data on a murine homologue. We show that human Lin28A binds miR-363 with 1:1 stoichiometry and with similar, if not higher, affinity (K_d = 16.6 ± 1.9 nM). Further analysis suggests that the interaction of the N-terminal cold shock domain of Lin28A with RNA is salt-dependent, supporting a model where the cold shock domain allows the protein to sample RNA substrates through transient electrostatic interactions.

Lin28 proteins are key post-transcriptional regulators of gene expression in higher eukaryotes.[1] They comprise two RNA binding domains: an N-terminal cold-shock domain (CSD) and a C-terminal Zinc Knuckle (ZnK) domain with two tandem CCHC-type zinc knuckles. This unique domain combination allows specific interactions with mRNAs and microRNAs (miRNAs) which contain conserved GGAG/GGUG motifs. [1–6] Due to these interactions, Lin28 has been implicated in pluripotency,[7–9] development,[10–13] alternative splicing,[4] metabolism[12, 14] and cancer[15–17]. Identifying Lin28 targets and characterising their interactions with Lin28 is therefore critical for understanding the molecular basis of Lin28-associated disorders.

The inhibition of let-7 family miRNA biogenesis by Lin28 has been widely studied. The binding of Lin28 to pre-let-7 in the cytoplasm prevents access of Dicer to its cleavage site. Further recruitment of terminal uridylyl transferase Zcchc11 results in the addition of a 3′ poly(U) tail, [6, 18] targeting the precursor RNA for degradation by the Dis3L2 nuclease.[19] A crystal structure of murine Lin28a in complex with let-7 RNA showed that the CSD binds the loop/pre-element/preE region of the miRNA while the ZnK domain contacts the GGAG motif (illustrated in Figure 1A). [20] Analysis of *Xenopus* Lin28b showed that the protein bound 83-nt *Xenopus*-pre-let-7f RNA with a K_d of 1.6 μM. [21] The same study showed that CSD remodels RNA structure to facilitate binding of the ZnK domain to the GGAG motif. More recent work with murine Lin28a suggested that the remodelling of RNA serves to expose additional sites for Lin28 binding, giving rise to 2:1 and 3:1 protein-RNA complexes, where effectively the protein shields pre-let-7 from Dicer.[22] An overall affinity of 0.13 nM was reported for such binding of Lin28 to a 46-nt let-7g substrate. [23]

Affinities of 1.7 and 0.29 nM were observed for 14-nt GAGG and GGAG-containing segments of this substrate, respectively. [22]

Among miRNAs outside of the let-7 family, several contain a 3′ GGAG motif and are targets of Lin28-dependent uridylation by Zcchc11. [6] In contrast, miR-363 of the 106~363 cluster, which also has this motif (Figure 1B) and a binding partner of Lin28, is not subjected to uridylation by Zcchc11, suggesting that its interaction with Lin28 is part of a previously uncharacterized regulatory pathway. Recently, a direct interaction between *Xenopus* Lin28 and the terminal loop of the precursor *Xenopus* -miR-363 was shown.[24] Contrary to what was observed for let-7 RNAs, knockdown of Lin28 in morphant embryos led to a decrease in mature miR-363 levels, suggesting an alternate function for Lin28 as a positive regulator of miR-363.

Previous studies of human Lin28 interaction with RNA were undermined by the unstable nature of this protein in the absence of bound nucleic acid. Here, we report a new strategy for producing stable, RNA-free, recombinant human Lin28. We show that the human protein binds both let-7g and miR-363 with high affinity in a 1:1 stoichiometry. We further show that this complex is resistant to changes in the ionic strength. In contrast, the CSD on its own binds in a manner highly dependent on ionic strength. These data suggest that the electrostatic properties of CSD play a major role in helping Lin28 search for RNA targets in the transcriptome.

EXPERIMENTAL PROCEDURES

Protein Production

The plasmid encoding the His-MBP-Lin28TT fusion protein (Figure 1C) was produced from the pETFF_2 plasmid provided by the York Technology Facility. The sequence encoding residues 32–187 of human Lin28A (*NCBI accession number NP_078950.1)* was amplified by PCR from a synthetic, codon optimized template (GeneArt). The pETFF_2 vector was linearized by PCR and purified by agarose gel electrophoresis. The Lin28 sequence was then inserted into the pETFF_2 vector using the In-Fusion ligation system (Clontech) and the product transformed into *E. coli*. Plasmid encoding the His-MBP-Lin28TT protein was transformed into the Rosetta2 (DE3) *E. coli* expression strain. Cells were grown in LB medium supplemented with 50 μM $ZnCl_2$ to an OD_{600} of 0.6. Expression was then induced by the addition of 1 mM IPTG, and cells were grown overnight at 16 °C. Cells were harvested and resuspended on ice in 50 mM Tris-Cl, pH 7.5, 150 mM NaCl, 2 mM β-mercaptoethanol, 10 μM $ZnCl_2$, 20 mM imidazole, and lysed by sonication. The lysate was applied to a Zn^{2+}-charged 5 mL HisTrap column (GE Healthcare) at 4 °C. The column was then washed for 16 h (0.1 mL/min flow rate) at 4 °C, with solution containing 50 mM MES, pH 6.0, 1 M NaCl, 2 mM β-mercaptoethanol, 10 μM $ZnCl_2$, 20 mM imidazole to remove nucleic acid contaminants. Bound proteins were eluted using 50 mM MES, pH 6.0, 1 M NaCl, 2 mM β-mercaptoethanol, 10 μM $ZnCl_2$, 500 mM imidazole. The eluted protein was applied to a S200 10/300 gel filtration column (GE Healthcare) in a solution containing 10 mM MES pH 6.0, 1 M NaCl, 2 mM β-mercaptoethanol, 10 μM $ZnCl_2$. Fractions containing the Lin28 fusion protein were concentrated and dialyzed against a solution containing 10 mM Tris-Cl, pH 7.5, 150 mM NaCl, 2 mM β-mercaptoethanol, 10 μM $ZnCl_2$, before being flash frozen in liquid nitrogen for storage.

RNA constructs

Unlabelled and 5′-fluorescein-labelled RNA corresponding to human let-7g and miR-363 (Figure 1D,E) were synthesized by Dharmacon. A cytosine was introduced to the 5′ end of the let-7g RNA for additional stability from base-pairing. A similar approach was taken in previous studies on murine let-7g RNA.[20]

SEC-MALLS

A Biosep SEC S3000 column (Phenomenex) was pre-equilibrated with 20 mM Tris pH 7.5 and 250 mM NaCl buffer and connected to a Dawn Helios II 18-angle light-scattering detector (Wyatt Technology). Lin28 fusion protein samples were diluted to 2 mg/mL (34 μM/38 μM for His-MBP-Lin28TT/His-MBP-CSD respectively) in buffer or buffer with equimolar amounts of RNA oligonucleotide. The eluting species were detected by measuring the UV absorbance at 280 nm, the concentration of the species was determined using an Optilab rEX refractometer (Wyatt Technology) and a refractive index increment of 0.185 mL/g was used for calculation of molecular weight in the ASTRA V software. Weight-average molecular weight values and the associated error of fit are reported.

Fluorescence Anisotropy

Titrations were performed using increasing concentrations of protein and 20 nM 5'-fluorescein-labelled RNA in 200 μL final volumes, in triplicate. The sample buffer contained 20 mM Tris-Cl pH 7.5, 50–750 mM NaCl, 10 mM β-mercaptoethanol, 50 μM $ZnCl_2$ and 0.01% (v/v) Tween20. Fluorescence readings were taken in a black flat-bottom 96-well plate (Nunc) at 25 °C in a BMG POLARstar Optima plate reader with detector gain set using an initial measurement of 20 nM free fluorescein in buffer. Dissociation constants for His-MBP-Lin28TT/RNA interactions were determined by fitting the following equation in Prism (GraphPad):

$$y = A_{\min} + (A_{\max} - A_{\min}) * \frac{\left((c + (x) + Kd) - \sqrt{(c + (x) + Kd)^2 - 4 * (x) * c}\right)}{2 * c}$$

where x is the concentration of protein in nM, y is the anisotropy (x1000), $A_{\min}$ is the anisotropy of free labelled RNA, $A_{\max}$ is the maximum anisotropy, c is the total concentration of labelled RNA (set to 20 nM) and K_d is the dissociation constant.

RESULTS

Human Lin28 fusion to MBP can be purified as a soluble, nucleic acid-free preparation

Initial attempts to produce nucleic acid-free human Lin28A as a His_6-fusion failed, as the protein quickly became lost on removal of nucleic acid with NaCl treatment (Figure S1). To improve solubility and stability, constructs were designed where Lin28A (residues 32–187, Lin28TT) or the CSD on its own (residues 32–127), were fused with His-tagged maltose-binding protein (His-MBP) via a three alanine peptide linker (Figure 1C). A long salt wash was included in the purification protocol to remove nucleic acid contaminants, which otherwise caused all protein to elute as a high molecule-weight protein-nucleic acid mixture during size-exclusion chromatography (Figure S2).

Human Lin28 forms 1:1 complexes with let-7g and miR-363

The His-MBP-Lin28TT fusion protein eluted in two steps during size exclusion chromatography: a sharp peak at 9.8 mL, corresponding to monomeric protein, with a weight-average molecular weight of 65 ± 4 kDa, determined by MALLS (theoretical mass, 59.5 kDa); and a broad peak in the void volume, indicating aggregation and

accounting for ~24% of eluting protein mass, calculated based on refractive index measurements.

Injecting equimolar amounts of His-MBP-Lin28TT and let-7g$^{29–57}$ RNA resulted in an earlier eluting peak relative to free monomeric protein and RNA (Figure 2A). An average molecular weight of 72 ± 1 kDa was determined, comparable to the theoretical mass of 68.4 kDa for a 1:1 protein:RNA complex.

The interaction of Lin28 with miR-363 was investigated using a 28-nt RNA segment, which includes the characteristic stem loop and the conserved GGAG motif (miR-363$^{19–46}$, Figure 1A,E). As with let-7g, an earlier eluting peak was observed for the protein-RNA mixture relative to free monomeric protein and RNA, with an observed molecular weight of 73 ± 2 kDa (Figure 2B). This agrees with the 68.8 kDa mass calculated for a 1:1 protein:RNA complex.

Lin28 binds let-7g and miR-363 with high affinity

The affinities of human Lin28 for let-7 RNA and miR-363 were subsequently measured. The fusion protein was titrated against a constant concentration of 5′ fluorescein-labelled let-7g$^{29–57}$ and miR-363$^{19–46}$ and changes in fluorescence anisotropy measured (Figure 2C,D). Equilibrium dissociation constants of 54.1 ± 4.2 nM and 16.6 ± 1.9 nM were deduced, respectively, under a 1:1 interaction model. No interaction was observed between the His-MBP tag and RNA (Figure S3). These data suggest that Lin28 binds let-7 RNA and miR-363 with comparable affinities.

Lin28 CSD forms higher-order species with let-7g and miR-363 RNA

To elucidate the role of the CSD in RNA binding, a His-MBP-CSD fusion protein was produced and its interactions with let-7g$^{29–57}$ and miR-363$^{19–46}$ studied. A significant peak in the void volume during size exclusion chromatography indicated that His-MBP-CSD has a strong tendency to aggregate, with approximately 76% of the eluting protein present in this peak (Figure 3). A peak corresponding to the 52-kDa monomeric protein could still be observed, with an experimental molecular weight of 52 ± 1 kDa. When mixed with let-7g or miR-363, a new peak corresponding to the complex was observed with average molecular weights of 76 ± 1 kDa and 72 ± 2 kDa, respectively (Figure 3). These values are between the expected molecular weights of 62 kDa and 113 kDa for a 1:1 and 2:1 protein-RNA complex, respectively. These data could be the result of protein aggregating while bound to RNA. Alternatively they may indicate that the CSD does not bind RNA in a strict 1:1 manner, in agreement with previous reports on murine Lin28 forming high-order complexes with RNA.[22] Contrasting with the relatively monodisperse 1:1 binding behaviour exhibited by the full-length protein, it can be proposed that the ZnK domain facilitates the formation of stable 1:1 complexes.

Lin28-miR363 complexes are insensitive to salt concentration

To determine if electrostatic forces have any role in the Lin28-miR-363$^{19–46}$ interaction, the fluorescence anisotropy experiments were repeated under different ionic strengths conditions. As the exact nature of the His-MBP-CSD:RNA complexes is not known, an appropriate model for data fitting could not be determined. However, the general trend in the affinity of the interaction can be seen qualitatively by

comparing anisotropy at different ionic strengths. The data show that for the two-domain His-MBP-Lin28TT protein, the affinity of the interaction remained relatively constant in all conditions (Figure 4A, Table S1). Conversely, the His-MBP-CSD/miR-363[19-46] interaction became weaker as the ionic strength of the buffer increased (Figure 4B), so much so that no binding was observed at 750 mM NaCl. These data show that unlike the two-domain protein, the CSD interaction with RNA is sensitive to the ionic strength. This implies that electrostatic interactions have a far greater role when the ZnK domain is not present.

DISCUSSION

Lin28 interacts with miR-363

The miR-363 miRNA was identified as a potential binding partner of Lin28, as the 3′ GGAG motif present in this sequence is highly conserved in land-based vertebrates. miR-363 is a member of the 106~363 miRNA cluster; a paralogous cluster to the 17~92 miRNA oncomir cluster.[30, 31] Recent reports have placed miR-363 as a putative tumour suppressor. In neuroblastoma cells, miR-363 expression inhibits colony formation, growth, invasion and metastasis through down regulation of the MYO1D and ADAM15 oncogenes.[32] miR-363 expression has been also linked with better prognosis and decreased metastatic potential in head and neck squamous cell carcinoma due to its targeting of podoplanin.[33] Expression of miR-363 also inhibits the growth of a cell line derived from a NK-cell lymphoma.[34] Given that both Lin28 and miR-363 are both implicated in the development of cancer, understanding the nature of Lin28/miR-363 interaction is of potential medical interest.

Previously reported K_d values for the interaction between Lin28 proteins and let-7 RNAs[20–23, 25, 26] display a large degree of variation, with differences over four orders

of magnitude. The reasons for such a large discrepancy are likely complex, and could be due to a range of factors including sample preparation, buffer conditions and the length and structure of the oligonucleotide tested.

Here, we show that the miR-363 RNA segment containing the characteristic stem loop followed by the GGAG motif forms a relatively stable complex with a human Lin28A fusion protein, with a K_d of 16.6 ± 1.9nM under the described conditions (Figure 2D). SEC-MALLS analysis indicates a 1:1 protein:RNA stoichiometry in the complex (Figure 2B). We also observe a 1:1 interaction with an equivalent segment of let-7g RNA (Figure 2A), in agreement with an earlier observation of a 1:1 complex made with an RNA oligonucleotide of similar length and secondary structure, derived from the terminal loop of *Mmu*let-7d.[20] Additionally, the K_d of 54.1 ± 4.2 nM of this interaction is comparable to the affinity of His-MBP-Lin28TT for the miR-363 RNA segment (Figure 2D). The data therefore indicate that Lin28 binds miR-363 and let-7 miRNAs in a similar manner.

This finding is of interest as the Lin28/miR-363 complex was shown to promote very little uridylation by Zcchc11 compared to let-7a-1.[6] In addition, the evidence of a direct interaction between amphibian Lin28 and miR-363, as well as the observation that knockdown of Lin28 results in decreased mature miR-363 levels, implies the alternative function of Lin28 as a positive regulator of miRNA biogenesis.[24] The results presented here show the similarities between the binding modes of let-7g and miR-363. Previously, it has been proposed that a change in the conformation of the 3′ terminus of the let-7g hairpin caused by Lin28 binding may facilitate the recruitment of the TUTase responsible for let-7g uridylation.[20] Differences in the conformations of bound miR-363 and let-7g would not be detectable by the methods employed here, but could account for the differences in the biological outcomes of Lin28 binding

through the recruitment of different downstream effectors. Further studies identifying factors that may interact with and influence binding of Lin28 to miRNA, as well as structural information on such assemblies, may be useful to further our understanding of this system.

Determinants of Lin28/RNA stoichiometry

A recent study demonstrated that Lin28 binds the let-7g 46-nucleotide stem loop segment in a stepwise manner, with up to 3 protein molecules per RNA.[22] Interactions were mediated by three RNA segments, containing an exposed loop of the let-7g stem loop or either the 5′-GGAG-3′ motif or its reverse (5′-GAGG-3′). The let-7g$^{29–57}$ oligonucleotide used here is shorter (29-nt) and only contains the 3′ GGAG motif. Likewise, the miR-363$^{19–46}$ and *Mmu*-let-7d RNA oligonucleotides contain only one GGAG motif, at the 3′ end. It is therefore possible that the stoichiometry of a Lin28/RNA complex is determined by: (1) the number of GGAG motifs present in the RNA, which determine the specific attachment to RNA; and (2) the length of the RNA, which determines the number of CSD molecules that can be accommodated on exposed single-stranded RNA regions.

Lin28 CSD guides RNA binding via electrostatic attraction

The structures of murine Lin28A in complex with let-7 family miRNA sequences,[20] and of the *Xenopus* Lin28B CSD domain,[21] show binding of the CSD to single stranded oligonucleotides through stacking interactions between the RNA bases and aromatic side chains on the CSD surface. In tandem, the ZnK domain binds the GGAG motif through a hydrogen bonding network, with a stacking interaction

formed between the side chain of Y140 and the bases of the final A and G of the motif.[20]

The sensitivity of the interaction of His-MBP-CSD with RNA to ionic strength (Figure 4B) implies that electrostatic forces play an equally important role in RNA binding. Examination of the CSD's electrostatic surface reveal clear areas of positive charge surrounding the nucleic acid binding site (Figure 4C). Apart from Lys95 (Lys92 in the human CSD), the phosphate groups seen in the structure are not directly contacted by these areas of positive charge. However, a major difference between the bacterial cold-shock protein homologues and the Lin28 CSD is the addition of two extra lysine residues to strand β4, which results in a more basic binding platform.[21] It is therefore possible that these areas of positive charge could fulfil a key role in attracting and guiding RNA to the binding site, facilitating the formation of base-specific hydrophobic and hydrogen-bond interactions as observed in crystal structures.

In conclusion, we propose that Lin28 uses its CSD to sample the transcriptome through transient electrostatic associations, similar to how DNA binding proteins locate their target sites through facilitated diffusion, by "sliding" and "hopping".[35–38] If Lin28 were to display a similar behaviour, it would increase the likelihood of ZnK binding to the short GGAG motif for stable complex formation. Depending on the structure and sequence of the RNA, melting and the association of further Lin28 molecules could then occur. Such a model may also have relevance in the light of recent work showing Lin28 can also bind to DNA and influence gene expression through the recruitment of epigenetic modification factors.[39] Future work will therefore need to elucidate Lin28's interaction with both the genome and transcriptome.

ACKNOWLEDGMENTS

We would like to thank Christoph Baumann for useful suggestions and Andrew Leech for help in conducting experiments.

REFERENCES

1. Huang, Y. (2012) A mirror of two faces: Lin28 as a master regulator of both miRNA and mRNA, *Wiley Interdiscip. Rev. RNA 3*, 483–494.

2. Cho, J., Chang, H., Kwon, S. C., Kim, B., Kim, Y., Choe, J., Ha, M., Kim, Yoon K., and Kim, V. N. (2012) LIN28A Is a suppressor of ER-associated translation in embryonic stem cells, *Cell 151*, 765–777.

3. Hafner, M., Max, K. E. A., Bandaru, P., Morozov, P., Gerstberger, S., Brown, M., Molina, H., and Tuschl, T. (2013) Identification of mRNAs bound and regulated by human LIN28 proteins and molecular requirements for RNA recognition, *RNA 19*, 613–626.

4. Wilbert, M. L., Huelga, S. C., Kapeli, K., Stark, T. J., Liang, T. Y., Chen, S. X., Yan, B. Y., Nathanson, J. L., Hutt, K. R., Lovci, M. T., Kazan, H., Vu, A. Q., Massirer, K. B., Morris, Q., Hoon, S., and Yeo, G. W. (2012) LIN28 binds messenger RNAs at GGAGA motifs and regulates splicing factor abundance, *Mol. Cell 48*, 195–206.

5. Mayr, F., and Heinemann, U. (2013) Mechanisms of Lin28-mediated miRNA and mRNA regulation—a structural and functional perspective, *Int. J. Mol. Sci. 14*, 16532–16553.

6. Heo, I., Joo, C., Kim, Y.-K., Ha, M., Yoon, M.-J., Cho, J., Yeom, K.-H., Han, J., and Kim, V. N. (2009) TUT4 in concert with Lin28 suppresses microRNA biogenesis through pre-microRNA uridylation, *Cell 138*, 696–708.

7. Yu, J., Vodyanik, M. A., Smuga-Otto, K., Antosiewicz-Bourget, J., Frane, J. L., Tian, S., Nie, J., Jonsdottir, G. A., Ruotti, V., Stewart, R., Slukvin, I. I., and Thomson, J. A. (2007) Induced pluripotent stem cell lines derived from human somatic cells, *Science 318*, 1917–1920.

8. Hanna, J., Saha, K., Pando, B., van Zon, J., Lengner, C. J., Creyghton, M. P., van Oudenaarden, A., and Jaenisch, R. (2009) Direct cell reprogramming is a stochastic process amenable to acceleration, *Nature 462*, 595–601.

9. Peng, S., Chen, L.-L., Lei, X.-X., Yang, L., Lin, H., Carmichael, G. G., and Huang, Y. (2011) Genome-wide studies reveal that Lin28 enhances the translation of genes important for growth and survival of human embryonic stem cells, *Stem Cells 29*, 496–504.

10. Yokoyama, S., Hashimoto, M., Shimizu, H., Ueno-Kudoh, H., Uchibe, K., Kimura, I., and Asahara, H. (2008) Dynamic gene expression of Lin-28 during embryonic development in mouse and chicken, *Gene Expression Patterns 8*, 155–160.

11. Faas, L., Warrander, F. C., Maguire, R., Ramsbottom, S. A., Quinn, D., Genever, P., and Isaacs, H. V. (2013) Lin28 proteins are required for germ layer specification in Xenopus, *Development 140*, 976–986.

12. Zhu, H., Shah, S., Shyh-Chang, N., Shinoda, G., Einhorn, W. S., Viswanathan, S. R., Takeuchi, A., Grasemann, C., Rinn, J. L., Lopez, M. F., Hirschhorn, J. N., Palmert, M. R., and Daley, G. Q. (2010) Lin28a transgenic mice manifest size and puberty phenotypes identified in human genetic association studies, *Nat. Genet. 42*, 626–630.

13. West, J. A., Viswanathan, S. R., Yabuuchi, A., Cunniff, K., Takeuchi, A., Park, I.-H., Sero, J. E., Zhu, H., Perez-Atayde, A., Frazier, A. L., Surani, M. A., and Daley, G. Q. (2009) A role for Lin28 in primordial germ-cell development and germ-cell malignancy, *Nature 460*, 909–913.

14. Zhu, H., Shyh-Chang, N., Segrè, A. V., Shinoda, G., Shah, S. P., Einhorn, W. S., Takeuchi, A., Engreitz, J. M., Hagan, J. P., Kharas, M. G., Urbach, A., Thornton, J. E., Triboulet, R., Gregory, R. I., Altshuler, D., and Daley, G. Q. (2011) The Lin28/let-7 axis regulates glucose metabolism, *Cell 147*, 81–94.

15. Viswanathan, S. R., Powers, J. T., Einhorn, W., Hoshida, Y., Ng, T. L., Toffanin, S., O'Sullivan, M., Lu, J., Phillips, L. A., Lockhart, V. L., Shah, S. P., Tanwar, P. S., Mermel, C. H., Beroukhim, R., Azam, M., Teixeira, J., Meyerson, M., Hughes, T. P., Llovet, J. M., Radich, J., Mullighan, C. G., Golub, T. R., Sorensen, P. H., and Daley, G. Q. (2009) Lin28 promotes transformation and is associated with advanced human malignancies, *Nat. Genet. 41*, 843–848.

16. Yang, X., Lin, X., Zhong, X., Kaur, S., Li, N., Liang, S., Lassus, H., Wang, L., Katsaros, D., Montone, K., Zhao, X., Zhang, Y., Bützow, R., Coukos, G., and Zhang, L. (2010) Double-negative feedback loop between reprogramming factor LIN28 and

microRNA let-7 regulates aldehyde dehydrogenase 1-positive cancer stem cells, *Cancer Res. 70*, 9463–9472.

17. Li, N., Zhong, X., Lin, X., Guo, J., Zou, L., Tanyi, J. L., Shao, Z., Liang, S., Wang, L.-P., Hwang, W.-T., Katsaros, D., Montone, K., Zhao, X., and Zhang, L. (2012) Lin-28 homologue A (LIN28A) promotes cell cycle progression via regulation of cyclin-dependent kinase 2 (CDK2), cyclin D1 (CCND1), and cell division cycle 25 homolog A (CDC25A) expression in cancer, *J. Biol. Chem. 287*, 17386–17397.

18. Hagan, J. P., Piskounova, E., and Gregory, R. I. (2009) Lin28 recruits the TUTase Zcchc11 to inhibit let-7 maturation in mouse embryonic stem cells, *Nat. Struct. Mol. Biol. 16*, 1021–1025.

19. Chang, H.-M., Triboulet, R., Thornton, J. E., and Gregory, R. I. (2013) A role for the Perlman syndrome exonuclease Dis3l2 in the Lin28-let-7 pathway, *Nature 497*, 244–248.

20. Nam, Y., Chen, C., Gregory, R. I., Chou, J. J., and Sliz, P. (2011) Molecular basis for interaction of let-7 microRNAs with Lin28, *Cell. 147*, 1080–1091.

21. Mayr, F., Schütz, A., Döge, N., and Heinemann, U. (2012) The Lin28 cold-shock domain remodels pre-let-7 microRNA, *Nucleic Acids Res. 40*, 7492–7506.

22. Desjardins, A., Bouvette, J., and Legault, P. (2014) Stepwise assembly of multiple Lin28 proteins on the terminal loop of let-7 miRNA precursors, *Nucleic Acids Res. 42*, 4615–4628.

23. Desjardins, A., Yang, A., Bouvette, J., Omichinski, J. G., and Legault, P. (2012) Importance of the NCp7-like domain in the recognition of pre-let-7g by the pluripotency factor Lin28, *Nucleic Acids Res. 40*, 1767–1777.

24. Warrander, F., Faas, L., Kovalevskiy, O., Peters, D., Coles, M., Antson, A. A., Genever, P., and Isaacs, H. V. (2016) Lin28 proteins promote expression of 17˜92 family miRNAs during amphibian development, *Dev. Dynam. 245*, 34–46.

25. Piskounova, E., Viswanathan, S. R., Janas, M., LaPierre, R. J., Daley, G. Q., Sliz, P., and Gregory, R. I. (2008) Determinants of microRNA processing inhibition by the developmentally regulated RNA-binding protein Lin28, *J. Biol. Chem. 283*, 21310–21314.

26. Piskounova, E., Polytarchou, C., Thornton, J. E., LaPierre, R. J., Pothoulakis, C., Hagan, J. P., Iliopoulos, D., and Gregory, R. I. (2011) Lin28A and Lin28B inhibit let-7 microRNA biogenesis by distinct mechanisms, *Cell 147*, 1066–1079.

27. Zuker, M. (2003) Mfold web server for nucleic acid folding and hybridization prediction, *Nucleic Acids Res. 31*, 3406–3415.

28. Motulsky, H., and Brown, R. (2006) Detecting outliers when fitting data with nonlinear regression - a new method based on robust nonlinear regression and the false discovery rate, *BMC Bioinformatics 7*, 123.

29. Loughlin, F. E., Gebert, L. F. R., Towbin, H., Brunschweiger, A., Hall, J., and Allain, F. H. T. (2012) Structural basis of pre-let-7 miRNA recognition by the zinc knuckles of pluripotency factor Lin28, *Nat. Struct. Mol. Biol. 19*, 84–89.

30. Landais, S., Landry, S., Legault, P., and Rassart, E. (2007) Oncogenic Potential of the miR-106-363 Cluster and its implication in human T-cell leukemia, *Cancer Res. 67*, 5699–5707.

31. He, L., Thomson, J. M., Hemann, M. T., Hernando-Monge, E., Mu, D., Goodson, S., Powers, S., Cordon-Cardo, C., Lowe, S. W., Hannon, G. J., and Hammond, S. M. (2005) A microRNA polycistron as a potential human oncogene, *Nature 435*, 828–833.

32. Qiao, J., Lee, S., Paul, P., Theiss, L., Tiao, J., Qiao, L., Kong, A., and Chung, D. H. (2013) miR-335 and miR-363 regulation of neuroblastoma tumorigenesis and metastasis, *Surgery 154*, 226–233.

33. Sun, Q., Zhang, J., Cao, W., Wang, X., Xu, Q., Yan, M., Wu, X., and Chen, W. (2013) Dysregulated miR-363 affects head and neck cancer invasion and metastasis by targeting podoplanin, *Int. J. Biochem. Cell Biol. 45*, 513–520.

34. Ng, S.-B., Yan, J., Huang, G., Selvarajan, V., Tay, J. L.-S., Lin, B., Bi, C., Tan, J., Kwong, Y.-L., Shimizu, N., Aozasa, K., and Chng, W.-J. (2011) Dysregulated microRNAs affect pathways and targets of biologic relevance in nasal-type natural killer/T-cell lymphoma, *Blood 118*, 4919–4929.

35. von Hippel, P. H., and Berg, O. G. (1989) Facilitated target location in biological systems, *J. Biol. Chem. 264*, 675–678.

36. Widom, J. (2005) Target site localization by site-specific, DNA-binding proteins, *Proc. Natl. Acad. Sci. U.S.A. 102*, 16909–16910.

37. Bonnet, I., Biebricher, A., Porté, P.-L., Loverdo, C., Bénichou, O., Voituriez, R., Escudé, C., Wende, W., Pingoud, A., and Desbiolles, P. (2008) Sliding and jumping of single EcoRV restriction enzymes on non-cognate DNA, *Nucleic Acids Res. 36*, 4118–4127.

38. Hammar, P. ,Leroy, P., Mahmutovic, A., Marklund, E. G., Berg, O.G., Elf, J. (2012) The lac repressor displays facilitated diffusion in living cells, *Science 336*, 1595–1598.

39. Zeng, Y., Yao, B., Shin, J., Kim, N., Song, Q., Liu, S., Su, Y., Guo, J. U., Huang, L., Wan, J., Wu, H., Qian, J., Cheng, X., Zhu, H., Ming, G.-l., Jin, P., and Song, H. (2016) Lin28A binds active promoters and recruits Tet1 to regulate gene expression, *Mol. Cell 61*, 153–160.

FIGURE LEGENDS

Figure 1. Lin28 and miRNA. (**A**) Architecture of Lin28 complex with miRNA.[(20)] (B) Alignment of pre-miR-363 sequences from several vertebrates. The conserved GGAG motif is highlighted (red box) and the region of the sequence corresponding to miR-363$^{19–46}$ segment used in this study designated in orange; segments of full-length mature miR-363 are designated in blue (5′) and green (3′). (C) Schematic of Lin28 constructs used in this study. Secondary structures of (D) let-7g$^{29–57}$ and (E) miR-363$^{19–46}$, predicted by MFOLD.[27]

Figure 2. Analysis of Lin28 interaction with RNA. SEC-MALLS analysis of protein, RNA and protein-RNA complex with elution profiles shown for (A) let-7g$^{29–57}$ and (B) miR-363$^{19–46}$. Fluorescence anisotropy analysis of Lin28 interaction with 5′-

fluorescein labelled (C) let-7g$^{29–57}$ and (D) miR-363$^{19–46}$ in 20 mM Tris-Cl pH 7.5, 100 mM NaCl, 10 mM β-mercaptoethanol, 50 μM $ZnCl_2$ and 0.01% (v/v) Tween20.

Figure 3. SEC-MALLS analysis of the His-MBP-CSD interaction with RNA. Elution profiles are shown for protein, RNA and protein-RNA complexes for (A) let-7g$^{29–57}$ and (B) miR-363$^{19–46}$.

Figure 4. Effect of ionic strength on Lin28 interaction with miR-363. Fluorescence anisotropy experiments were conducted using fluorescein labelled miR-363$^{19–46}$ at different ionic strengths with increasing concentrations of (A) His-MBP-Lin28TT or (B) His-MBP-CSD. (C) Model of human CSD complex with RNA based on atomic structures of human Lin28b CSD (PDB entry 4A4I) and *Xenopus* Lin28b CSD/RNA complex (PDB entry 4A75). The electrostatic surface potential for the human CSD, from -1 V (red) to +1 V (blue).

Supporting Information. Figure S1. Protein stability following removal of nucleic acid with salt treatment. Figure S2. Purification of His-MBP-Lin28TT. Figure S3. Fluorescence anisotropy analysis of His-MBP with RNA. Table S1. Equilibrium dissociation constants of the His-MBP-Lin28TT-miR-363$^{19–46}$ interaction at different NaCl concentrations, as measured by fluorescence anisotropy.

Figure 1

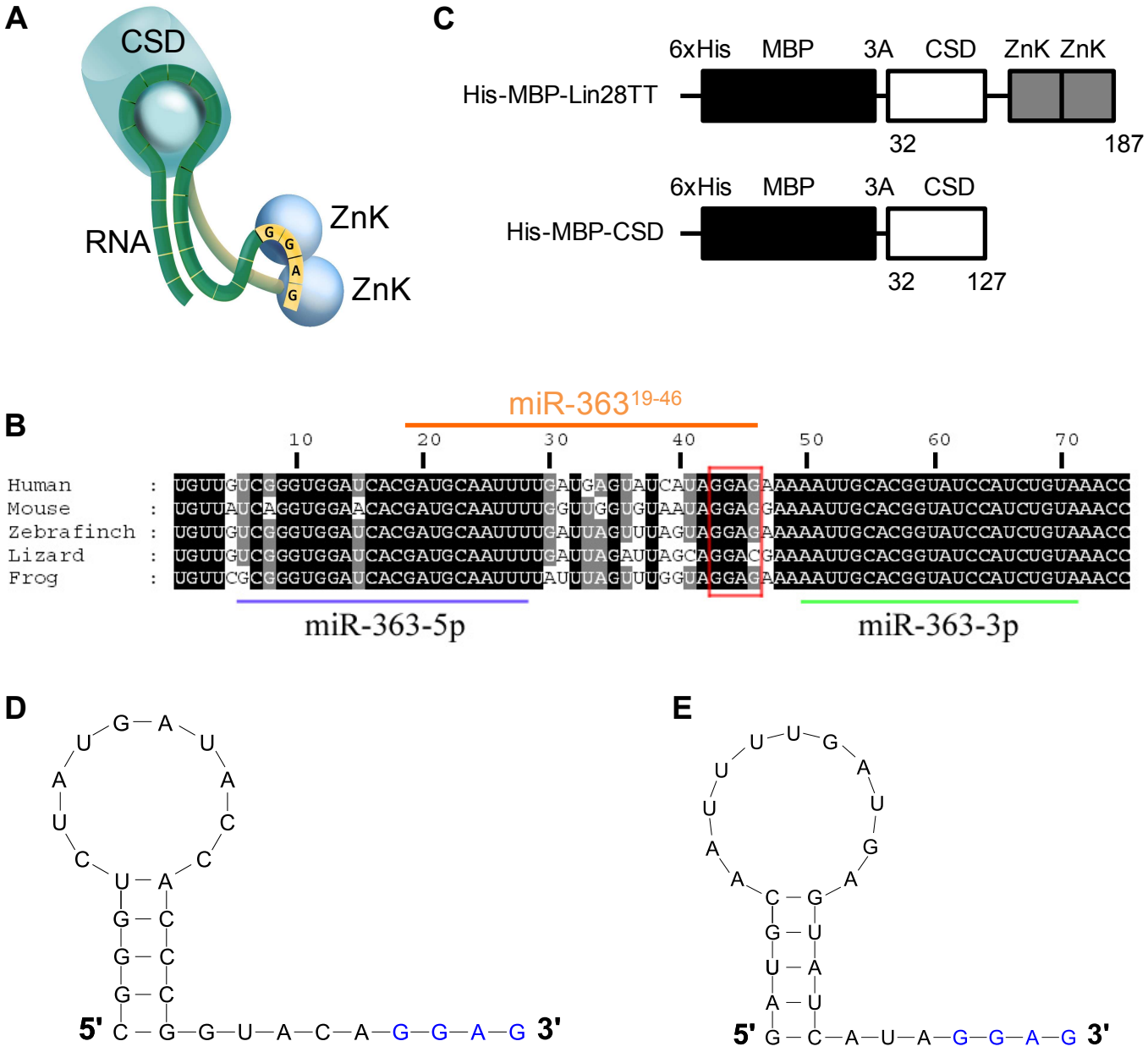
A
CSD
RNA
ZnK
ZnK
G
G
A
G
C
6xHis
MBP
3A
CSD
ZnK
ZnK
His-MBP-Lin28TT
32
187
6xHis
MBP
3A
CSD
His-MBP-CSD
32
127
B
miR-363 19-46
10
20
30
40
50
60
70
Human :
Mouse :
Zebrafinch :
Lizard :
Frog :
miR-363-5p
miR-363-3p
D
5' C G G U A C A G G A G 3'
E
5' G C A U A G G A G 3'

Figure 2

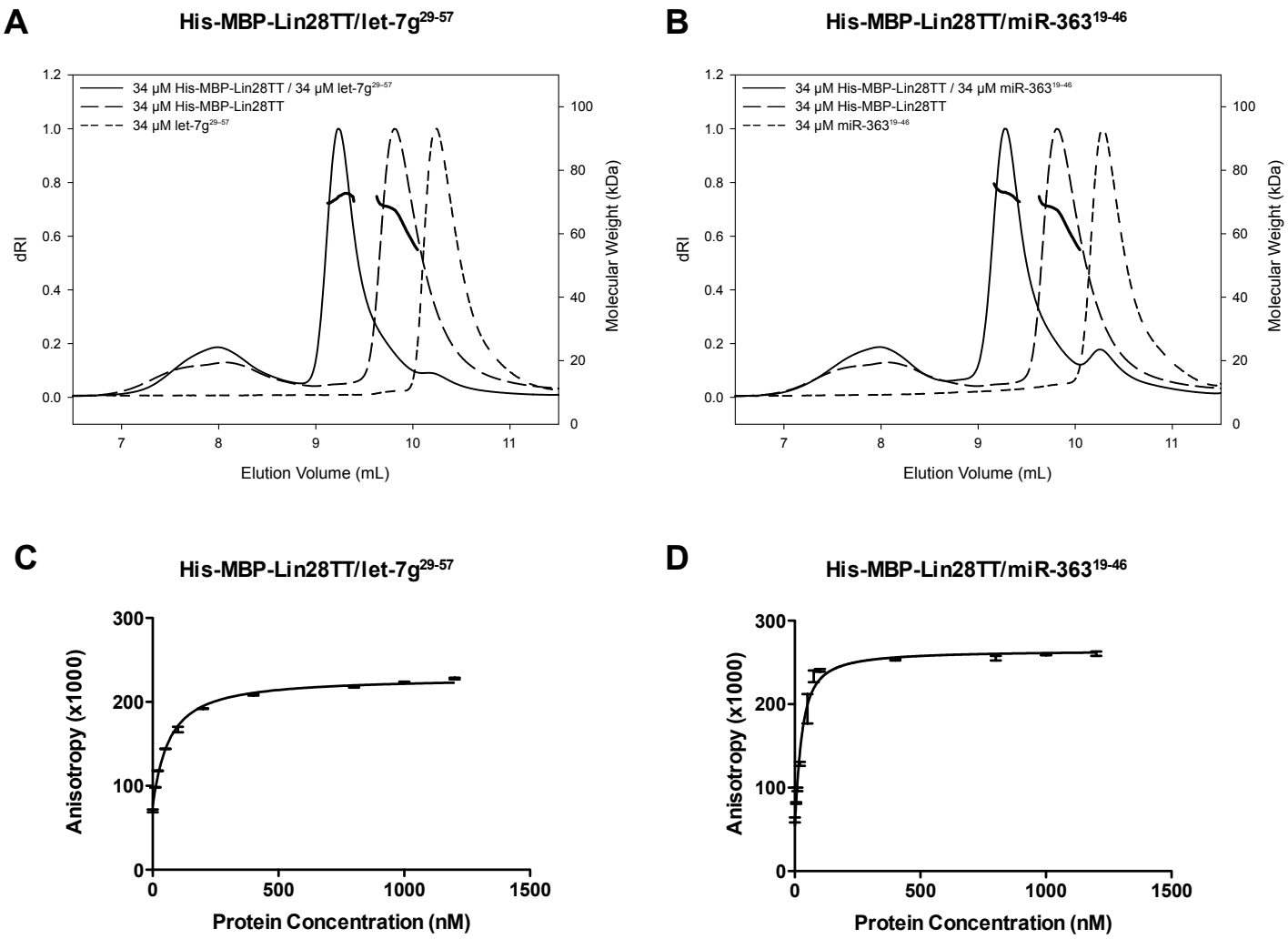
A
His-MBP-Lin28TT/let-7g29-57
34 μM His-MBP-Lin28TT / 34 μM let-7g29–57
34 μM His-MBP-Lin28TT
34 μM let-7g29–57
dRI
Molecular Weight (kDa)
Elution Volume (mL)
B
His-MBP-Lin28TT/miR-36319-46
34 μM His-MBP-Lin28TT / 34 μM miR-36319–46
34 μM His-MBP-Lin28TT
34 μM miR-36319–46
dRI
Molecular Weight (kDa)
Elution Volume (mL)
C
His-MBP-Lin28TT/let-7g29-57
Anisotropy (x1000)
Protein Concentration (nM)
D
His-MBP-Lin28TT/miR-36319-46
Anisotropy (x1000)
Protein Concentration (nM)

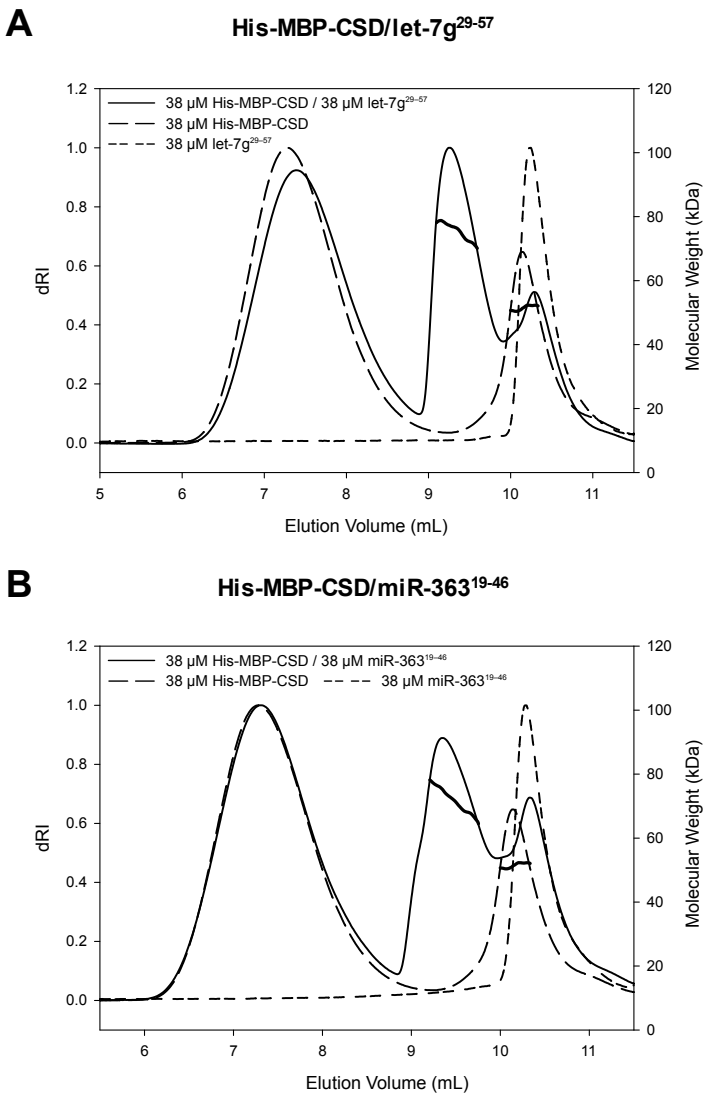
A
His-MBP-CSD/let-7g29-57
38 μM His-MBP-CSD / 38 μM let-7g29–57
38 μM His-MBP-CSD
38 μM let-7g29–57
dRI
Molecular Weight (kDa)
Elution Volume (mL)
B
His-MBP-CSD/miR-36319-46
38 μM His-MBP-CSD / 38 μM miR-36319–46
38 μM His-MBP-CSD
38 μM miR-36319–46
dRI
Molecular Weight (kDa)
Elution Volume (mL)

Figure 4

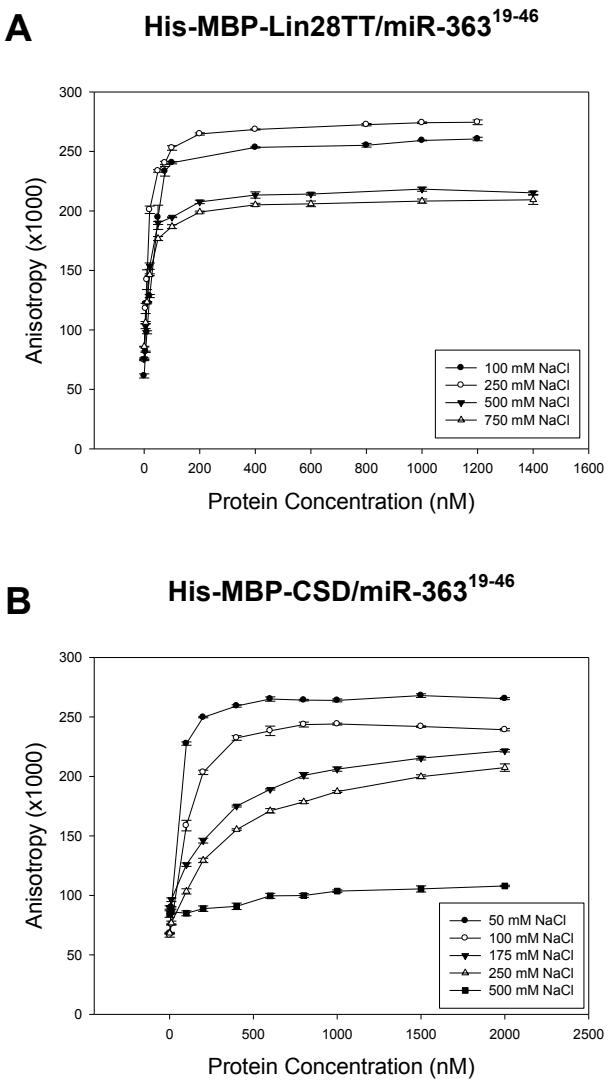
A
His-MBP-Lin28TT/miR-363[19-46]
Anisotropy (x1000)
Protein Concentration (nM)
100 mM NaCl
250 mM NaCl
500 mM NaCl
750 mM NaCl
B
His-MBP-CSD/miR-363[19-46]
Anisotropy (x1000)
Protein Concentration (nM)
50 mM NaCl
100 mM NaCl
175 mM NaCl
250 mM NaCl
500 mM NaCl
C